Modelling Swash Zone Hydrodynamics Using Discontinuous Galerkin Finite Element Method

W. Aboulatta[1], N. Dodd [2], R. Briganti[3], T.H.M.A. Kasem[4], and M.A.F. Zaki[5]

[1]Ph.D., Faculty of Engineering, University of Nottingham, NG7 2RD, UK. Corresponding author email: Waddaa.Aboulatta@eng.cu.edu.eg

[2]Professor of Coastal Dynamics, Faculty of Engineering, University of Nottingham, NG7 2RD, UK.

[3]Associate Professor, Faculty of Engineering, University of Nottingham, NG7 2RD, UK.

[4]Associate Professor, Faculty of Engineering, Cairo University, Giza, Egypt

[5]Professor of Engineering Mechanics, Faculty of Engineering, Cairo University, Giza, Egypt

ABSTRACT

A 2D numerical model for the solution of the Nonlinear Shallow Water Equations (NSWEs) using the Discontinuous Galerkin Finite Element Method (DGFEM) is presented. A new adaptation of the thin film approach is developed for the wetting/drying treatment. The model is applied to a number of test cases that can be characterized as swash flows, or as cases that are particularly useful for swash flow modelling. The DGFEM model shows robustness and provides accurate predictions of water depth, velocities, and shoreline movement. For the case of bore collapse on a plane beach the model performs well against a state-of-the-art finite volume swash code. The new wetting/drying algorithm is tested against a previous algorithm within the same framework for simulating a solitary wave propagating on a beach with bottom friction, showing a noticeable improvement in the shoreline prediction. The model is also tested against a more subtle test case, including generation of subharmonic edge waves, in order to test the effectiveness of DGFEM in reproducing second order effects. The model simulates the excitation and development of the

sub-harmonic edge waves when compared to the analytical solutions in the literature. Overall, it is shown here for the first time that the DGFEM technique can be used to simulate accurately a wide range of swash zone flows and therefore swash zone processes.

INTRODUCTION

The swash zone is the zone of the beach that is alternately covered and uncovered by water, and extends from the limit of run-down to the limit of run-up. Fluid and sediment interactions occurring in this region cause the erosion and accretion of the beach and define landward boundary conditions for large-scale nearshore/coastal hydrodynamics and morphodynamics. In fact, swash processes determine whether sediment is stored on the upper beach or instead is returned to the surf zone and potentially transported offshore (Bakhtyar et al. 2009; Chardón-Maldonado et al. 2016). As such, accurate and robust numerical models of the swash zone are very important for coastal scientists and engineers.

Swash flows are a distinct category of flows that result from a wind wave impinging on a sloping beach. Swash flows can either be of non-breaking or breaking waves. For non-breaking waves the wave reflects and the crest and trough of the wind wave are distorted into an anti-node of the resulting standing wave that correspond to the maximum run-up and run-down respectively, the difference between which corresponds to half the shoreline amplitude. If a breaking wave (i.e. a bore) impinges on a sloping beach the bore collapses at the shoreline, and the wave energy is converted to onshore water velocity. In this case the maximum run-up depends on the shoreline velocity and the beach slope, and the whole resulting swash flow, which is free from the wave motion that created it, lasts for a swash period. Non-breaking swash flows are distinguished from wetting/drying tidal motions on the same beach in that the cross-shore (depth-integrated) dynamics of tides on a sloping beach are almost entirely described by mass conservation (Pritchard and Hogg 2003), whereas both mass and momentum balances play a significant role for wind waves. Tsunami-driven bore-collapse flows are distinguished from their wind wave counterparts in that wind wave periods are typically not too dissimilar to the swash period (Baldock and Holmes 1999); tsunamis, in contrast, are sometimes single events, and often result in overwash and debris flows

rather than typical swash backwash. Note also that on mildly sloping beaches, the swash period of an individual wave is so long that it almost never is completed. Instead there are infragravity motions of the shoreline, corresponding to wave groupiness (see e.g. Mase 1995). Hereafter we refer to swash flows as that sub-category of wetting/drying flows that satisfy the above criteria.

Non-linear shallow water equations (NSWEs) are often used to model swash-zone hydrodynamics (Hubbard and Dodd 2002; Brocchini et al. 2001; Borthwick et al. 2006). Finite Volume Methods (FVMs) have been one of the most favoured methods during the last decades for simulating swash-zone hydrodynamics (Briganti et al. 2016; Rogers et al. 2003). FVMs are successful in allowing easy implementation of unstructured grids, which are useful for describing complex topography, and allowing, via so-called slope/flux limiters (LeVeque 2002), an efficient movement between 1^{st} and 2^{nd} order accuracy so as to avoid the development of spurious oscillations that can develop at discontinuities in 2^{nd} order schemes.

Continuous Galerkin finite element methods (CGFEMs) are relatively unexplored for swash problems. In general, CGFEMs can be computationally more demanding when compared to FVMs (for a similar cell/element density), but their strength is the combination of accuracy, versatility, and robustness. Nonetheless CGFEMs remain inherently limited at shocks and other discontinuities. This has prompted the development of Discontinuous Galerkin FEMs (DGFEMs). The DGFEM applied to the NSWEs provides an approach that combines the advantages of both CGFEM (potentially higher order accuracy) and FVMs (good shock-capturing properties). The DGFEM has been shown to reasonably accurately simulate solutions for some wetting/drying flows: the solution for a periodic, non-breaking wave on a beach of Carrier and Greenspan (1958) (see Bunya et al. 2009); the transient solution of Carrier and Greenspan (1958) (see Duran et al. 2013; Duran and Marche 2014); the case of inundation of a tsunami (solitary wave) on a bay due to Zelt (1986) (see Duran and Marche 2014). DGFEM has also been shown to simulate accurately a 2D solution for a wetting/drying flow in a parabolic basin: the periodic, curved-surface solution of Thacker (1981) (see Bunya et al. 2009; Ern et al. 2008; Karna et al. 2011; Kesserwani et al. 2018; Gourgue et al. 2009; Lai and Khan 2012; Lee and Lee 2016; Wen et al. 2016); a 1D, flat-free-surface

solution of Thacker (1981) (see Marras et al. 2018; Kesserwani and Liang 2010); a revolving, 2D flat-surface solution of Thacker (1981) (see Duran et al. 2013). These solutions, though not swash flows, are demanding (particularly the less well-studied latter), and therefore a good test of robustness of the modelling, particularly if velocities are examined. Finally, an experimental test case (Briggs et al. 1995) for tsunami run-up on a conical island has been examined using DGFEM (see Duran et al. 2013). In addition, estuarine flows at field scale have been examined (Brus et al. 2019; Le Bars et al. 2016; Dawson et al. 2011; de Brye et al. 2010; Karna et al. 2011; Mulamba et al. 2019; Gourgue et al. 2009). Despite their importance in coastal engineering, infragravity and edge waves solutions have not been used to test DGFEM solvers, to the knowledge of the authors. Analytical and highly accurate numerical solutions for this problem exist (see Özkan-Haller and Kirby 1997) and they are particularly suited to show how dissipative NSWE solvers are. For this reason edge waves are simulated here to fill this gap in research.

In this paper we present a DGFEM model of the 2D NSWEs, and apply it to a variety of swash flows, and a specific case that is particularly helpful for swash flow modelling. The purpose is to provide the first such comprehensive application of DGFEM to the representative range of these flows to assess the capability of DGFEM for this kind of modelling. In doing so we also verify a new 2D DGFEM model. This model is mostly based on existing approaches–and is thus representative of mainstream DGFEMs–although with an extended wetting/drying algorithm. To this end we re-test two cases listed above, which have both only been examined in one previous study, and present four cases not previously examined using DGFEMs. We consider here only analytical or quasi-analytical NSWE test cases, because tests against laboratory or field data provide tests of the accuracy of the NSWEs to simulate the flow rather than of the numerical approach to solve the NSWEs.

The paper is organized as follows. Section 2 gives the governing equations and Section 3 introduces the numerical model. Section 4 verifies the model against a number of analytical and quasi-analytical solutions; the choices for each case are explained in the relevant subsections. Finally, conclusions are presented.

THE 2D NON-LINEAR SHALLOW WATER EQUATIONS:

The 2D NSWEs written in the flux conservative form are :

$$\frac{\partial \vec{\boldsymbol{W}}_i}{\partial t} + \nabla . \boldsymbol{F}_i(\vec{\boldsymbol{W}}) = \vec{\boldsymbol{S}}_i(\vec{\boldsymbol{W}}) \ , \tag{1}$$

where i = 1, 2, or 3 and $\vec{\boldsymbol{W}}_i$ is the ith component of the vector $\vec{\boldsymbol{W}}$ of conserved variables:

$$\vec{\boldsymbol{W}} = [h, uh, vh]^T \ , \tag{2}$$

where h is the water depth, u and v are the depth averaged velocity components in x and y directions. $\boldsymbol{F}_i$ is the vector comprising the ith row of the flux function matrix whose columns are the flux function vectors $\vec{\boldsymbol{f}}_x$, $\vec{\boldsymbol{f}}_y$:

$$\boldsymbol{F} = [\vec{\boldsymbol{f}}_x \ \vec{\boldsymbol{f}}_y] = \begin{bmatrix} uh & vh \\ u^2h + \dfrac{gh^2}{2} & uvh \\ uvh & v^2h + \dfrac{gh^2}{2} \end{bmatrix} . \tag{3}$$

$\vec{\boldsymbol{S}}_i$ is the ith component of the vector $\vec{\boldsymbol{S}}$ of source/sink terms, which is given by

$$\vec{\boldsymbol{S}} = \left[0, \quad -gh\frac{\partial z_b}{\partial x} - \frac{\tau_x}{\rho}, \quad -gh\frac{\partial z_b}{\partial y} - \frac{\tau_y}{\rho}\right]^T \ , \tag{4}$$

where z_b is the bed level, so that the water level $\eta = z_b + h$, g is the gravitational acceleration, ρ is the water density, and where τ_x, τ_y are the bed shear stresses in the x, y directions defined as:

$$\tau_x = \rho c_d u\sqrt{u^2 + v^2}, \quad \tau_y = \rho c_d v\sqrt{u^2 + v^2} \ , \tag{5}$$

where c_d is a dimensionless bed friction coefficient. See Figure 1 for a schematic depiction of the variables.

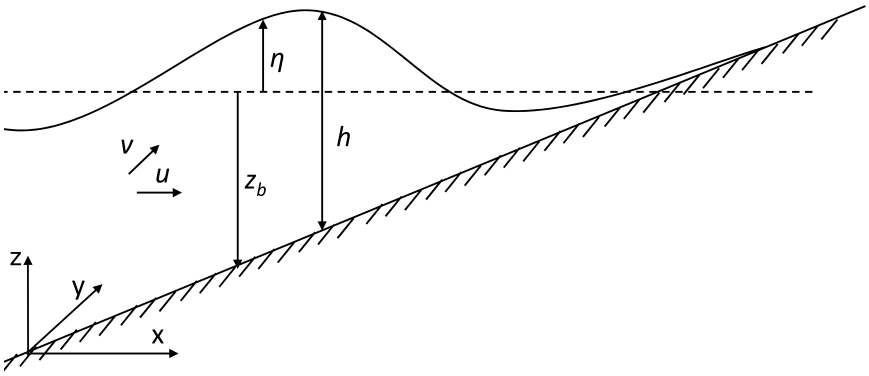

Fig. 1. A schematic depiction of independent and dependant variables.

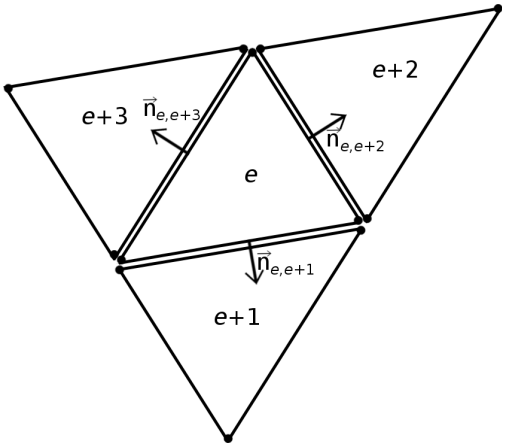

Fig. 2. Geometry of DGFEM domain, depicting triangular element e, neighboring elements (e+1, e+2, e+3); and outward normal vectors for e.

NUMERICAL METHODOLOGY

The domain is discretized into a set of non-overlapping elements. An unstructured grid is used to realise the full potential of DGFEM. Triangular elements are used here, these being the most commonly used unstructured elements (Kubatko et al. 2006; Aizinger and Dawson 2002; Kubatko et al. 2009). The boundary of the element e is denoted by ∂e (see Figure 2 for a sketch).

In order to obtain the discrete integral form of the NSWEs, we first replace the physical dependent variables h, uh, vh by approximated functions: $h_e, (uh)_e, (vh)_e$ defined on each element

e, as e.g.:

$$h_e = \sum_{i=1}^{3} \phi_i h_i \tag{6}$$

where h_i is the variable (in this case water depth) value at node i, and ϕ_i is the shape function (Li 2006). Accordingly we can replace $\vec{\boldsymbol{W}}$ by $\vec{\boldsymbol{W}}_e$. Note that here we use a first order approximation, to investigate what is achievable without the benefit of higher order accuracy. These approximated functions are allowed to be discontinuous across the element boundaries. Multiplying (1) by the shape function vector $\vec{\phi} = [\phi_1,\ \phi_2,\ \phi_3]^T$ and integrating over each element e (Li 2006), we obtain:

$$\int_e \vec{\phi} \left(\frac{\partial \vec{\boldsymbol{W}}_{e_i}}{\partial t} + \nabla . \boldsymbol{F}_i(\vec{\boldsymbol{W}}_e) - \vec{\boldsymbol{S}}_i(\vec{\boldsymbol{W}}_e) \right) dA = 0 \, . \tag{7}$$

Then, integrating the second term by parts and applying Green's theorem (Li 2006), we obtain

$$\int_e \vec{\phi} \frac{\partial \vec{\boldsymbol{W}}_{e_i}}{\partial t} \, dA - \int_e \nabla \vec{\phi} . \boldsymbol{F}_i(\vec{\boldsymbol{W}}_e) \, dA + \int_{\partial e} \vec{\phi} (\boldsymbol{F}_i(\vec{\boldsymbol{W}}_e) . \vec{\boldsymbol{n}}_{e,e+k}) \, ds = \int_e \vec{\phi} \vec{\boldsymbol{S}}_i(\vec{\boldsymbol{W}}_e) \, dA \, , \tag{8}$$

where $\vec{\boldsymbol{n}}_{e,e+k}$ is the local outward normal unit vector on the element e boundary that faces element $e + k$ ($k = 1, 2, 3$; see Figure 2).

Numerical Flux at Element Boundary

The flux $\boldsymbol{F}_i(\vec{\boldsymbol{W}}_e) . \vec{\boldsymbol{n}}_{e,e+k}$ may be dual-valued across the element boundary ∂e_{e+k} due to the fact that discontinuities are allowed across the element boundary ∂e. Therefore, it needs to be replaced with a single valued numerical flux function $\hat{\boldsymbol{F}}_i$:

$$\int_e \vec{\phi} \frac{\partial \vec{\boldsymbol{W}}_{e_i}}{\partial t} \, dA - \int_e \nabla \vec{\phi} . \boldsymbol{F}_i(\vec{\boldsymbol{W}}_e) \, dA + \int_{\partial e} \vec{\phi} \hat{\boldsymbol{F}}_i \, ds = \int_e \vec{\phi} \vec{\boldsymbol{S}}_i(\vec{\boldsymbol{W}}_e) \, dA \, . \tag{9}$$

The standard Roe Flux (Roe 1981) representation of $\hat{\boldsymbol{F}}$ is used:

$$\hat{\boldsymbol{F}} = \frac{1}{2} \left[\boldsymbol{F}_n(\vec{\boldsymbol{W}}_e^{(\partial e_{e+k})}) + \boldsymbol{F}_n(\vec{\boldsymbol{W}}_e^{(\partial (e+k)_e)}) \right] - \frac{1}{2} \hat{\boldsymbol{K}} |\hat{\boldsymbol{\Lambda}}| \hat{\boldsymbol{K}}^{-1} \left(\vec{\boldsymbol{W}}_e^{(\partial e_{e+k})} - \vec{\boldsymbol{W}}_e^{(\partial (e+k)_e)} \right) \tag{10}$$

where $\vec{\boldsymbol{W}}_e^{(\partial e_{e+k})}$ are the dependent variables calculated at the boundary of the element e that faces

the element $e + k$, and $\boldsymbol{F}_n$ is a vector whose ith component is defined by

$$\boldsymbol{F}_{n_i} = \boldsymbol{F}_i.\vec{\boldsymbol{n}}_{e,e+k}. \tag{11}$$

$\boldsymbol{K}$ is the matrix:

$$\boldsymbol{K} = \begin{bmatrix} 1 & 0 & 1 \\ u - \sqrt{gh}n_x & -n_y & u + \sqrt{gh}n_x \\ v - \sqrt{gh}n_y & n_x & v + \sqrt{gh}n_y \end{bmatrix}, \tag{12}$$

whose columns are eigenvectors of the normal Jacobian matrix:

$$\boldsymbol{J}_n = \boldsymbol{J}_x n_x + \boldsymbol{J}_y n_y, \tag{13}$$

where n_x, n_y are the x, y components of the outward normal unit vector $\vec{n}_{e,e+k}$ and

$$\boldsymbol{J}_x = \frac{\partial \vec{\boldsymbol{f}}_x}{\partial \vec{\boldsymbol{W}}} = \begin{bmatrix} 0 & 1 & 0 \\ gh - u^2 & 2u & 0 \\ -uv & v & u \end{bmatrix}, \tag{14}$$

$$\boldsymbol{J}_y = \frac{\partial \vec{\boldsymbol{f}}_y}{\partial \vec{\boldsymbol{W}}} = \begin{bmatrix} 0 & 0 & 1 \\ -uv & v & u \\ gh - v^2 & 0 & 2v \end{bmatrix}. \tag{15}$$

Finally,

$$|\boldsymbol{\Lambda}| = \begin{bmatrix} |\lambda_1| & 0 & 0 \\ 0 & |\lambda_2| & 0 \\ 0 & 0 & |\lambda_3| \end{bmatrix}, \tag{16}$$

where λ_1,λ_2, and λ_3 are the eigenvalues of $\boldsymbol{J}_x$:

$$\lambda_1 = un_x + vn_y - \sqrt{gh}, \tag{17}$$

$$\lambda_2 = un_x + vn_y, \tag{18}$$

$$\lambda_3 = un_x + vn_y + \sqrt{gh}, \tag{19}$$

and where u, v, and h are Roe-averaged values (Roe 1981).

Time Integration

Using the methodology of the previous subsections the equations can now be written as a system of ODE's,

$$\frac{d}{dt}(\boldsymbol{W}_{e_i}) = F(\boldsymbol{W}_{e_i}). \tag{20}$$

For time integration here we apply a first order (Euler) scheme,

$$\boldsymbol{W}_{e_i}^{n+1} = \boldsymbol{W}_{e_i}^{n} + \Delta t F(\boldsymbol{W}_{e_i}^{n}), \tag{21}$$

where $\boldsymbol{W}^n = \boldsymbol{W}(t_0 + \sum_{i=1}^{n} \Delta t_i)$, t_0 is the initial time, and Δt_i is the time interval for integration. Since this is an explicit scheme, therefore the time step must be limited by a Courant–Friedrichs–Lewy (CFL) stability condition (Kubatko et al. 2006), here:

$$\Delta t \leq min\left(\frac{l_e}{\lambda_e(2p+1)}\right), \tag{22}$$

where l_e is the minimum distance between two nodes in the element e, λ_e is an estimate of the maximum absolute value of the eigenvalues for the element e, and p is the order of the approximation functions (Kubatko et al. 2006).

Using a linear shape functions for spatial approximation in the DGFEM approach (second order accuracy O(Δx^2)) may result in non-physical oscillations. To circumvent this problem, the scheme must satisfy the Total Variation Diminishing (TVD) criterion (Harten 1983), which here is achieved

by using a minmod slope limiter (Li 2006).

Wetting/Drying Treatment

A so-called thin film approach in the framework of DGFEMs (Bunya et al. 2009) is used for the treatment of the wetting/drying front. Generally, when the mean of the water depth, within an element e, $h_e < h_{min}$ (minimum threshold), that element is marked as dry and the velocity there is set to zero. So a thin film of water is preserved all over the domain even in "dry" elements. The advantages of the thin film approach are that it provides a good balance between the accuracy of the solution and the computational cost (Bunya et al. 2009); in principle, this avoids the need for shoreline tracking and it can be adopted to ensure the positivity of water depth. An algorithm of this type was used previously with DGFEM by Bunya et al. (2009) with some success. However, to ensure more robust performance and to minimize the computational cost, particularly for the very dynamic shoreline behavior considered here, a new adaptation is developed.

The wetting/drying treatment is applied at the end of each time step in conjunction with a slope limiting process. In pseudo code it can be described as:

1. If $h_i \geq h_{min}$, for all nodes of the element e, then e is wet and will not undergo the wetting/drying treatment, instead it will undergo slope limiting.
2. Else, if $(h_1+h_2+h_3)/3 \geq h_{min}$, then e is still considered wet and the new updated variables are:

$$h_{1_{new}} = h_{2_{new}} = h_{3_{new}} = (h_1 + h_2 + h_3)/3 \,, \tag{23}$$

$$(uh)_{1_{new}} = (uh)_{2_{new}} = (uh)_{3_{new}} = ((uh)_1 + (uh)_2 + (uh)_3)/3 \,, \tag{24}$$

$$(vh)_{1_{new}} = (vh)_{2_{new}} = (vh)_{3_{new}} = ((vh)_1 + (vh)_2 + (vh)_3)/3 \,. \tag{25}$$

3. Else, if $(h_1 + h_2 + h_3)/3 > 0$, then this element is considered dry and the new updated

variables are:

$$h_{1_{new}} = h_{2_{new}} = h_{3_{new}} = (h_1 + h_2 + h_3)/3, \tag{26}$$

$$(uh)_{1_{new}} = (uh)_{2_{new}} = (uh)_{3_{new}} = 0, \tag{27}$$

$$(vh)_{1_{new}} = (vh)_{2_{new}} = (vh)_{3_{new}} = 0. \tag{28}$$

4. Else, this element has negative water depths and is reset :

$$h_{1_{new}} = h_{2_{new}} = h_{3_{new}} = 0.95h_{min}, \tag{29}$$

$$(uh)_{1_{new}} = (uh)_{2_{new}} = (uh)_{3_{new}} = 0, \tag{30}$$

$$(vh)_{1_{new}} = (vh)_{2_{new}} = (vh)_{3_{new}} = 0. \tag{31}$$

This approach conserves mass, as long as the average water depth inside the element $(h_1 + h_2 + h_3)/3 > 0$, and momentum, unless $(h_1 + h_2 + h_3)/3 < h_{min}$. Also during element calculations, to prevent any non-physical processes, the flux between dry elements is set to zero. It should be noted that this approach can yield the seemingly anomalous result that negative depths at all nodes are reset to $0.95h_{min}$ (via condition 4), whereas nodal depths such that $h_{min} > (h_1 + h_2 + h_3)/3 > 0$, will be reset to potentially much smaller (but still positive) values (via condition 3). In practice this appears not to be a problem.

Absorbing-generating boundary conditions

Here we implement a 1D absorbing-generating boundary condition following Kobayashi et al. (1987). Kobayashi et al. (1987) used the method of characteristics to predict the reflected wave height at the off-shore boundary; by adding it to the imposed incident wave height, an approximate total wave height can be attained. The absorbing-generating boundary allows the numerical model to simulate realistic hydrodynamic processes in the swash zone by absorbing the beach reflected waves at the seaward boundary and modifying the input signal at the boundary taking into account the reflected waves.

VERIFICATION TESTS

A number of test cases are undertaken, presented here in order of increasing demand on the model performance.

The periodic solution of Carrier-Greenspan (1958)

The model is tested against the analytical periodic solution of Carrier and Greenspan (1958), hereinafter CG58. This is a 1D case of a perfectly reflected normally incident monochromatic wave on a sloping beach. As mentioned, this case has been examined in an earlier study (Bunya et al. 2009) using DGFEM, but we retain it here because of its importance for swash problems. Here we choose an incoming wave amplitude $a = 0.00475$ m at the seaward end of the domain ($x = 0$), wave period $T = 8$ s, domain length $L = 10$ m. This is equivalent to a non-dimensional amplitude (A in CG58) of $A = 0.8$. This amplitude corresponds to $4A_{shore}$, where A_{shore} is the non-dimensional amplitude at the shoreline. Note that for $A = 1$ then the wave has a vertical gradient at the shoreline (i.e., it is at the threshold of breaking), so $A = 0.8$ is considered a demanding case to simulate because the free surface gradient near the shore is large. The minimum drying threshold was set to $h_{min} = 10^{-4}$m. The element size, in addition to the shoreline water depth gradient ($dh(x_s)/dx$), influence h_{min} such that the smallest h_{min} that can be used is restricted by the element size and the shoreline water depth gradient ($dh(x_s)/dx$). It was found in most cases that $h_{min} = 10^{-4} - 10^{-5}$ m is sufficient to achieve the convergence in the shoreline trajectory results.

The domain is discretized into a row of triangular elements such that $\Delta x \approx \Delta y \approx 0.0025$m, and the model is run for seven wave periods (with average $\Delta t = 1.5 \times 10^{-4}$s) to make sure that the numerical solution reaches a steady state. The water level and depth averaged velocity are plotted every one eighth of the wave period in Figures 3a and 3b. These Figures show small discrepancies near the shoreline between the analytical solution and the present model results for water level and bigger ones for depth averaged velocity. These results are consistent with those observed by Hubbard and Dodd (2002) (using finite volume methods); the errors visible in Figure 3b are consistent with–although a little larger than–those observed by Hubbard and Dodd (2002) (who also use adaptive grid refinement), for $A = 1$. Bunya et al. (2009) give results in terms of discharge

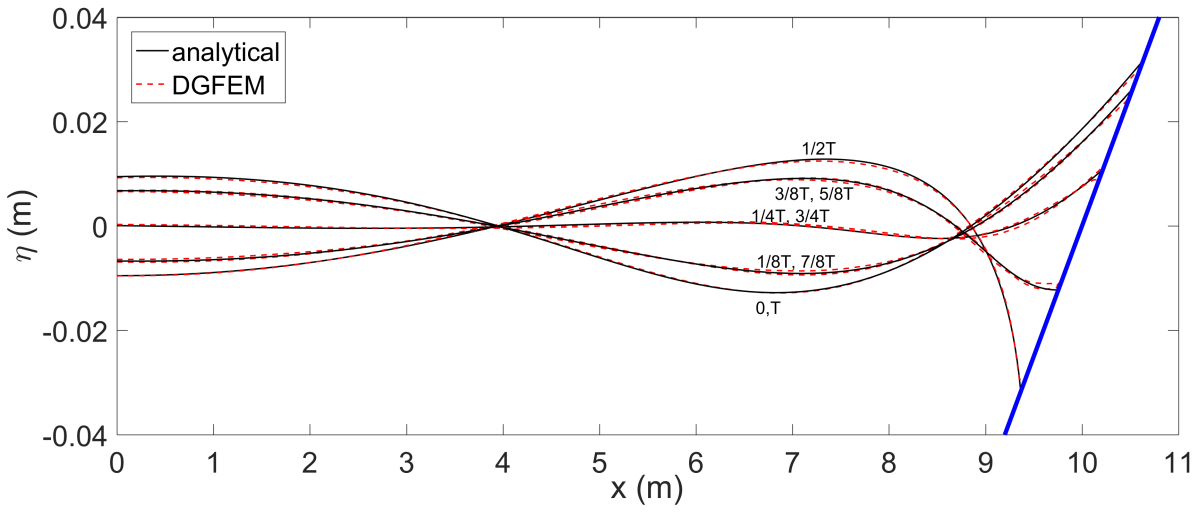

(a)

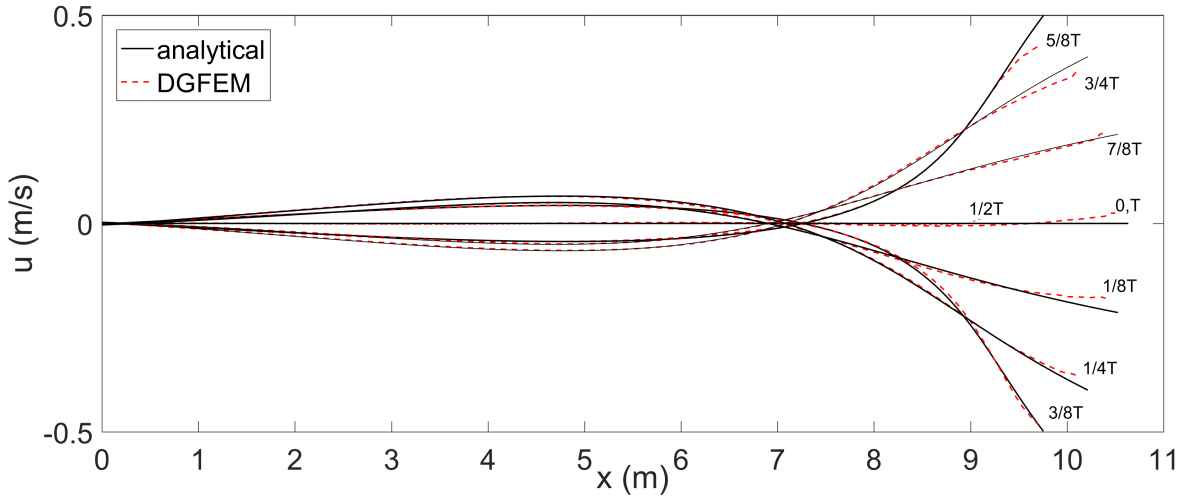

(b)

Fig. 3. Free surface elevation (a) and velocity (b) over one period (the seventh period) for $A = 0.8$ for the periodic CG58 solution (see text for other model parameters). Results plotted every one eighth of the wave period.

rather than u, but results shown in Figure 3a seem consistent with those of Bunya et al. (2009) (it is not clear what value of A was used therein). Figures 4a and 4b also show consistent agreement, this time between the analytical solution and model results for both the off-shore boundary and the moving shoreline $x_s = x_s(t/T)$. The model performance for the velocity at the shoreline is assessed

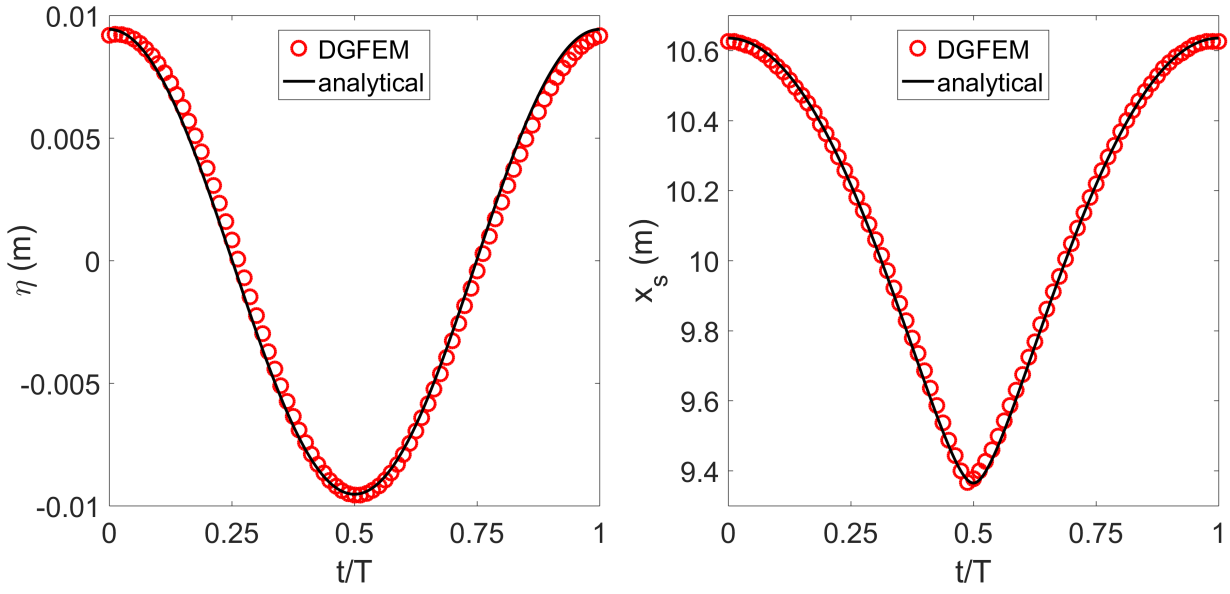

Fig. 4. Free surface elevation at (a) the offshore boundary, and (b) shoreline position, from the DGFEM model for the periodic CG58 solution ($A = 0.8$) over one period (the seventh). Both plotted against their analytical equivalents.

by computing the Root Mean Squared Error (RMSE) for u_s. The RMSE is generally defined as:

$$RMSE = \sqrt{\frac{\sum_{i=1}^{n}(f_{the} - f_{num})^2}{n}} \tag{32}$$

where f_{num} is a generic numerically predicted variable and f_{the} is the theoretical value of the same variable, n is the number of time steps in a swash cycle. Here we compute RMSE for the variable $u_s/\sqrt{gh_o}$, which for the case at hand is 0.0160. Furthermore, a series of 20 periods for the incident wave was simulated here and it was confirmed that the performance of the model, quantified by RMSE of the water depth, remained essentially unmodified in time, indicating that cumulative errors are negligible.

Bore collapse at the shoreline

The analytical solution of Shen and Meyer (1963) describes a bore collapse event at the shoreline, and has not so far been examined using a DGFEM description. The solution of Shen and Meyer

	$\epsilon_{run-up}(\%)$		
Δx	$h_{min} = 10^{-6}$ m	$h_{min} = 10^{-7}$ m	$h_{min} = 10^{-8}$ m
0.04m	5.1	1.8	0.2
0.02m	5.5	1.05	-0.8
0.01m	5.55	1.7	-1.85
0.001m	8.05	5.47	2.49
0.005m	8.8	5.75	4.1

TABLE 1. ϵ_{run-up} for 15 different simulations.

(1963) was subsequently extended by Peregrine and Williams (2001) to the whole swash, who also introduced the dam-break description. Therefore, because we use a dam-break on the slope as our initial condition we refer to this solution as the PW01 event hereafter. The case is more demanding than that of CG58 because a very thin film of water must be reproduced in the swash motion, and because of the supercritical flow in much of the swash. This test is also an extreme case because, in the absence of bed friction, there is a zero shoreline water depth gradient ($dh(x_s)/dx = 0$) for $t > 0$. It is also an important case for swash motions, because it serves as a test for a wide variety of swash flows in which the swash period is typically a little shorter than the wave period, which is typical of many steeper beaches, as well as some coastal protection structures.

The initial conditions for the PW01 event comprise $h = 1$ m for $x \leq 0$ and $u \equiv 0$, with $x = 0$ being the dam position, and bed slope $\tan\beta = 0.1$. A series of numerical experiments are carried out to find the grid size and h_{min} combination that offers best agreement with the analytical solution. Following the work of Briganti and Dodd (2009), here we calculate the run-up percentage error ϵ_{run-up},

$$\epsilon_{run-up} = \frac{x_{s,max,ana} - x_{s,max,num}}{x_{s,max,ana}} \times 100, \tag{33}$$

where $x_{s,max,ana}, x_{s,max,num}$ are the maximum horizontal extent for the run-up of the analytical and numerical solution, respectively. Table 1 shows ϵ_{run-up} for 15 different tests.

The combination $\Delta x = 0.04$ m, $h_{min} = 10^{-8}$ m produces the smallest ϵ_{run-up}, while $\Delta x = 0.02$ m, $h_{min} = 10^{-7}$ m produces the best general agreement with the quasi-analytical solution of Zhu and Dodd (2013) (Figure 5). Note that, the non-monotonic behaviour of ϵ_{run-up} was also observed

	ϵ_{run-up} (%)	
Simulation data	Present model	Briganti and Dodd (2009)
$\Delta x = 0.04$ m, $h_{min} = 10^{-6}$ m	5.1	≈ 8.5
$\Delta x = 0.04$ m, $h_{min} = 10^{-7}$ m	1.8	≈ 7.75
$\Delta x = 0.02$ m, $h_{min} = 10^{-6}$ m	5.5	≈ 5.75
$\Delta x = 0.02$ m, $h_{min} = 10^{-7}$ m	1.05	≈ 5.25

TABLE 2. ϵ_{run-up} comparison between the present model results and Briganti and Dodd (2009).

in FVM models, e.g. see Fig.12 in Briganti and Dodd (2009). This behaviour is because the PW01 event possesses zero depth gradient at the shoreline. So, for fixed Δx, decreasing h_{min} means that more of the tip region can be represented, which implies a smaller ϵ_{run-up}. For the same reason decreasing Δx for fixed h_{min} does not always improve the resolution of the tip modelling; instead this just increases the number of cells near the (incorrect) wet-dry boundary, in which water depth only just exceeds h_{min}, and therefore in which wetting-drying algorithms in general impose only approximate solutions (e.g. preserve mass only).

The second combination offers better agreement with the analytical solution for the water depth contours, shoreline location during the backwash, and depth averaged velocity contours (especially near the shoreline). However, it produces a slightly higher ϵ_{run-up} than other combinations. Table 2 shows a comparison between the errors produced using grids ($\Delta x = 0.02$ m,$h_{min} = 10^{-6}$ m and $\Delta x = 0.04$ m, $h_{min} = 10^{-7}$ m) and that produced by Briganti and Dodd (2009) (these errors are computed by interpolating the values in their figures). For all simulations, the present model produced significant lower ϵ_{run-up} with respect to the cited model. For this case RMSE for $u_s/\sqrt{gh_0}$ is 0.0275.

The shock solution of Antuono (2010)

Antuono (2010) introduced an analytical solution for the case of a shock approaching a plane beach. The well known case of Shen and Meyer (1963) can be considered a particular case of this general solution (Antuono 2010). Therefore, this offers a good test for the present model. To find this solution, Antuono (2010) chooses the boundary condition such that the incoming Riemann invariant is constant at the offshore boundary (for more details, see Antuono 2010). At

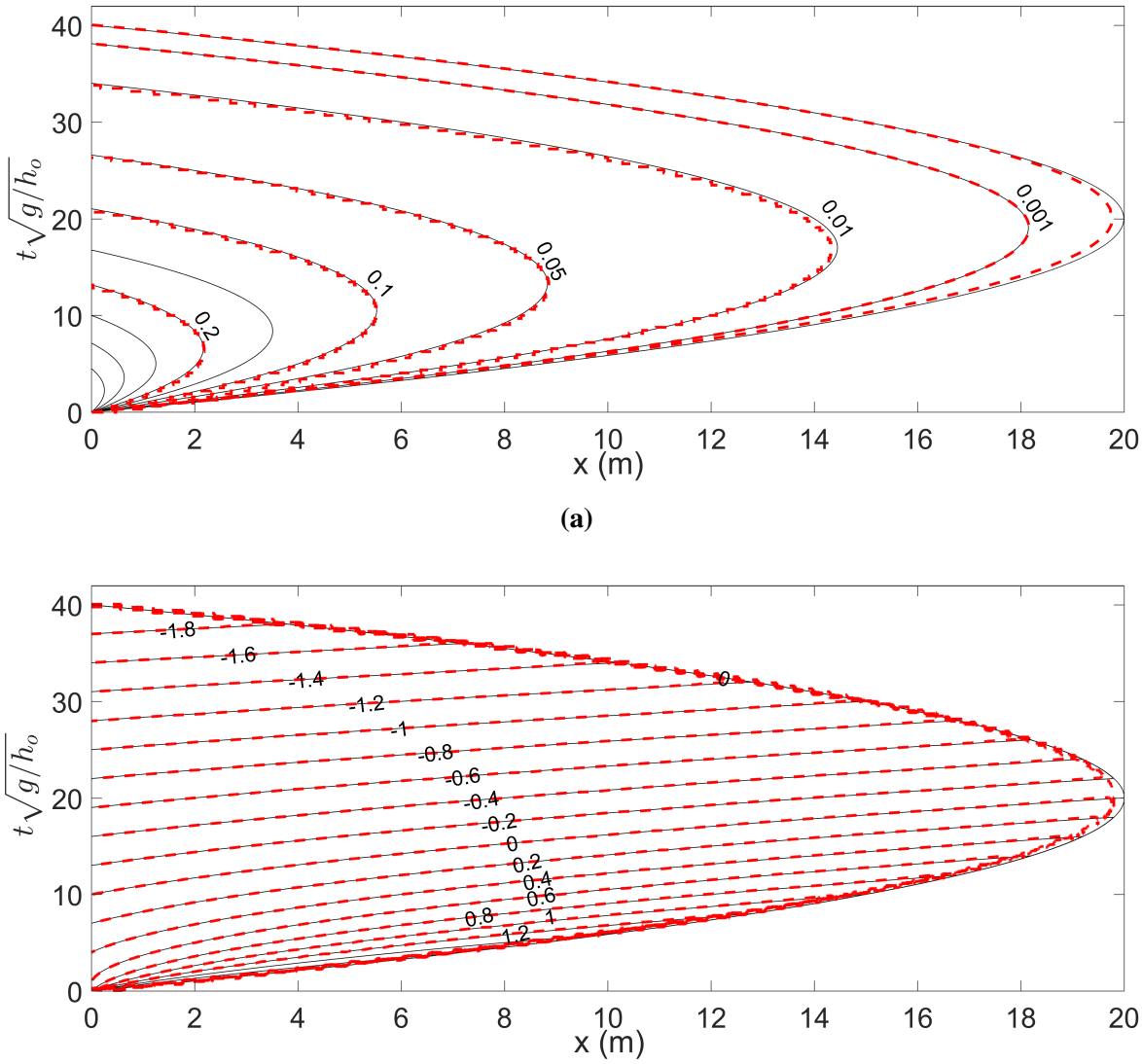

Fig. 5. PW01 event, contour plot showing comparison between quasi-analytical solution (black lines) and DGFEM using $\Delta x = 0.02$ m and $h_{min} = 10^{-7}$ m (red dashed lines), $h_o = 1$ m; (a) h contours, and (b) u contours.

the off-shore boundary $u_i = 0.15\sqrt{gh_o} - 0.5g \tan\beta\, t$ and the incoming Riemann invariant is set to $2u_i + 2\sqrt{gh_o} + g \tan\beta\, t$, where u_i is the incident wave velocity at the off-shore boundary, $\tan\beta$ is the bed slope, and h_o is the water depth at the offshore boundary. Here we choose $\tan\beta = 0.1$ and $h_o = 1$ m. The numerical domain is discretized into a row of triangular elements with $\Delta x = 0.005$ m, and the minimum drying threshold is set to $h_{min} = 10^{-5}$ m.

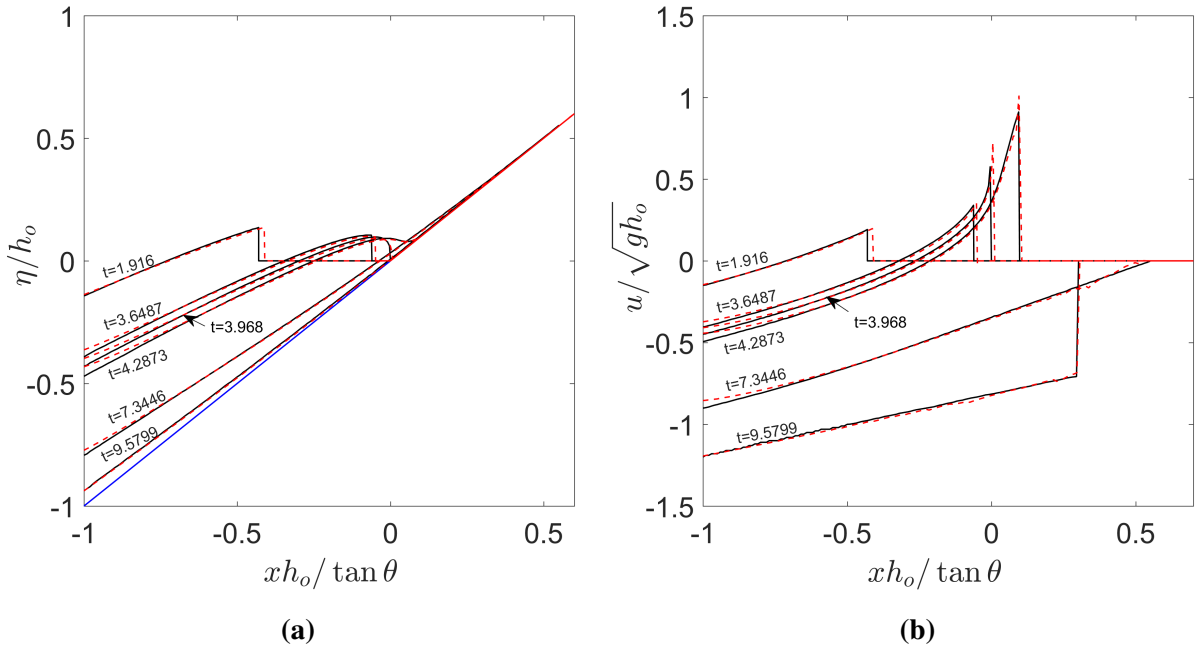

Fig. 6. Antuono (2010) case; black solid lines - analytical solution, red dashed lines - present model results; (a) Water level, (b) Flow velocity.

Figure 6 shows the model results at six different instants compared to the analytical solution of Antuono (2010). The model results showed faster shock propagation at first, then the numerical and analytical solutions gradually catch up. Nonetheless, the model predictions have maximum run-up error $\epsilon_{run-up} = 3.1\%$, which indicates good agreement with the analytical solution. Further quantification of the performance of the model is given by the RMSE for $u_s/\sqrt{gh_0}$, which is 0.0202.

Solitary wave over a frictional beach

This case is introduced to test the wetting/drying algorithm behaviour on a frictional beach, to compare its performance against a previous similar algorithm (Bunya et al. 2009), and to show the present model performance in simulating more realistic swash zone events. This case is described by solitary wave of wave height $H_w = 0.6$ m on still water depth at the offshore boundary $h_o = 1$ m, where $x = 0$ is the still water shoreline location, and the bed friction coefficient is $c_d = 0.01$. The reference solution for this case is provided by the model of Zhu and Dodd (2015), which, for this

case, solves the NSWEs on a fixed bed using the method of characteristics and shock conditions. The reader is referred to the aforementioned paper for more details. The domain/case description consists of two regions; i) for $x \leq -10$ m: the bed is flat (zero bed slope), and the the water level is described by $h(x \leq -10, t = 0) = 1 + H_w \text{sech}^2(0.3((3H_w)/(4h_o^3))^{1/2}(x + 22))$ and the water velocity is described by $u(x \leq -10, t = 0) = 2\sqrt{gh(x \leq -10, t = 0)} - 1$, and ii) for $x > -10$ m: $\tan\beta = 0.0667$ and the flow is at rest. The domain is discretized into a row of triangular elements with $\Delta x = 0.04,\ 0.01$ m, and the minimum drying threshold is set to $h_{min} = 10^{-3}$ and 10^{-7} m, respectively. The time required for the runs was 1 and 35 minutes, respectively. Note that the model uses parallel processing over GPU, and the computing was carried out on a pc with GTX680M GPU, a 2.6 GHz i7 CPU, and 8GB of RAM. These two combinations were chosen to show the results when more computational practical values are used, and to show the model ability to provide accurate predictions while simulating very small depths.

A comparison between the quasi-analytical solution, the present model results with the new wetting/drying algorithm, and the present model results with the wetting/drying algorithm introduced by Bunya et al. (2009) is shown in Figure 7. It is worth mentioning that Bunya et al. (2009) introduced an additional stability criteria to ensure the conservation of both mass and momentum while using their wetting/drying algorithm. This increases the model run time by a factor of 10 in our implementation of the method. However, the inspection of the results while not using it showed negligible loss of mass. Hence, here we choose saving the run time over conserving the mass and the momentum. Two different grid and minimum drying threshold combination were used for the comparison. The model results for $\Delta x = 0.01$ m, $h_{min} = 10^{-7}$ m has maximum run up error $\epsilon_{run-up} = 4.1\%$ using the new presented wetting/drying algorithm and $\epsilon_{run-up} = 5\%$ when Bunya et al. (2009) wetting/drying algorithm is used. Both algorithms results for $h_{min} = 0.001$ m showed less accurate shoreline predictions, with maximum run-up error $\epsilon_{run-up} = 4.2\%$ (new wetting/drying algorithm) and 5.2% (Bunya et al. 2009). Nonetheless, all other water depth results (for both algorithms) are well reproduced (Figure 7).

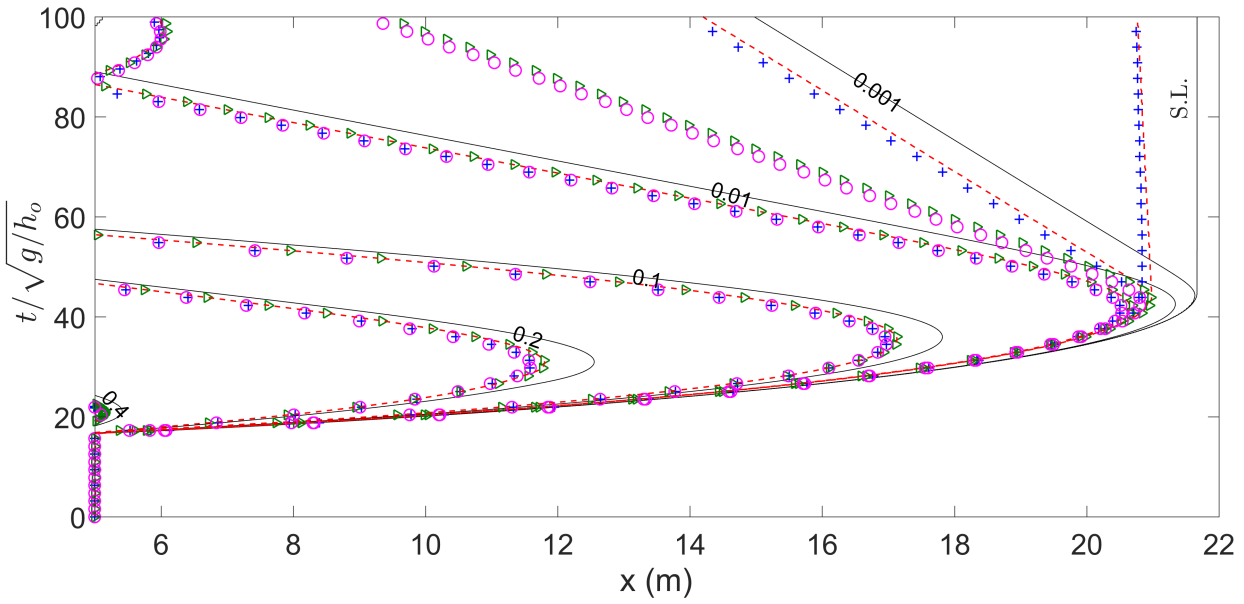

Fig. 7. Solitary wave; water depth contours comparison between; quasi-analytical solution (black lines), the present model results using the presented wetting/drying scheme (Δx = 0.04 m, h_{min} = 10^{-3} m - green triangle symbols; Δx = 0.01 m, h_{min} = 10^{-7} m - red dashed lines), Bunya et. al. (2009) wetting/drying algorithm (Δx = 0.04 m, h_{min} = 10^{-3} m - magenta circle symbols; Δx = 0.01 m, h_{min} = 10^{-7} m - blue plus symbols).

Sub-harmonic edge wave generation

The final test has also never been addressed using DGFEM. It is chosen to examine the ability of DGFEM to capture more subtle, second order motions within the NSWEs, which a dissipative numerical model might fail to reproduce. A good test of this type is that first conducted by Özkan-Haller and Kirby (1997) in which a normally incident monochromatic wave train impinges on a plane frictionless beach, without breaking, thus forming a standing wave. As such the solution is like that of CG58. However, this wave is unstable to alongshore perturbations with the wavelength of sub-harmonic edge waves (Guza and Davis 1974), which because the simulation has an alongshore and cross-shore extent, should be evident in the simulation if the dynamics are faithfully captured. To ensure a non-breaking wave, an incident wave amplitude a_i = 0.025 m and wave period T_i = 10 s are chosen. This a_i is larger than that used by Özkan-Haller and Kirby (1997) (a_i = 0.01 m), to ensure that a_i is significantly bigger than the drying threshold used by the present model during the simulation (h_{min} = 0.005m). For the domain, the bed slope $\tan\beta$ = 0.1, as in Özkan-Haller and

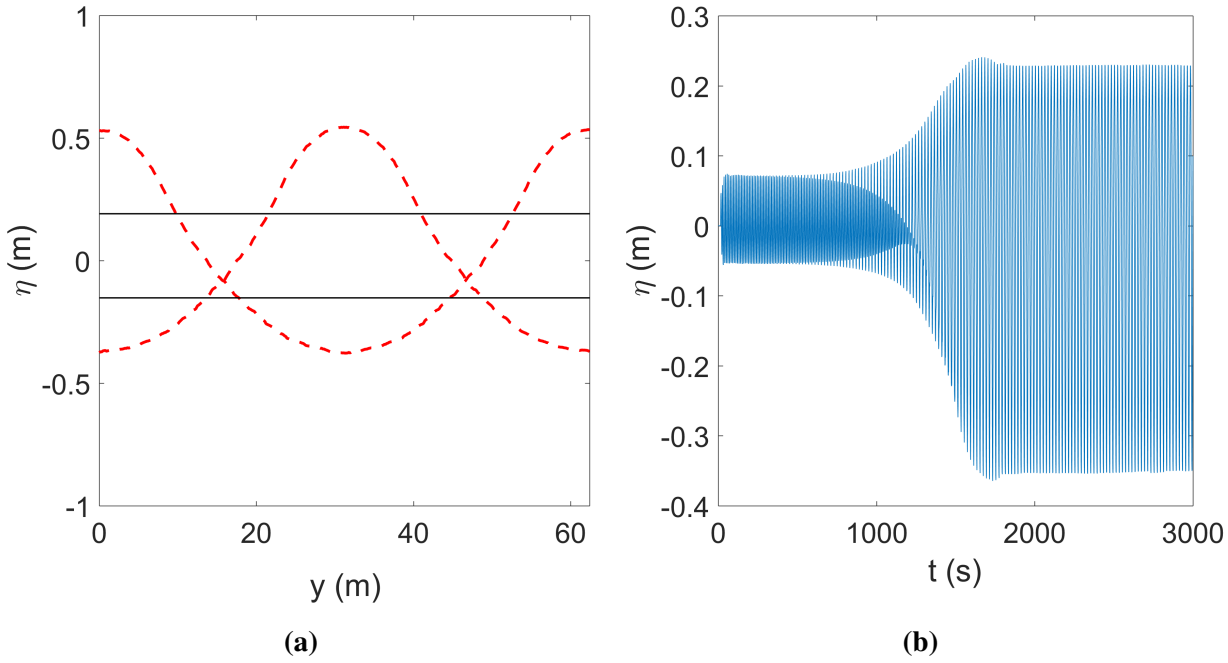

Fig. 8. Sub-harmonic edge wave generation; (a) $\eta(x_s(y,t))$ ($x_s(y,t)$ is the shoreline position) at the maximum run-up and maximum run-down over the whole domain, before edge wave excitation (black lines), and after the edge wave is fully developed (red dashed lines), (b) η at 6m away from still water shoreline.

Kirby (1997), and the still water shoreline is 100 m from the offshore boundary. The domain width is 62.43 m. This domain width is equivalent to the wavelength (λ_{sub}) of a sub-harmonic edge wave of period 20 s (Rockliff 1978):

$$\left(\frac{\omega_i}{2}\right)^2 = (2m+1)g\tan\beta\frac{2\pi}{\lambda_{sub}} \tag{34}$$

where $\omega_i = 2\pi/T_i$ is the incident wave angular frequency, and m is the edge wave mode. The grid is divided into two parts: swash zone with $\Delta x \approx \Delta y \approx 0.06$m and the rest of the domain with $\Delta x \approx \Delta y \approx 1$m. Free lateral boundary conditions (i.e., a border of "ghost" elements in which the independent variable (h, u, v) is set to that from the adjacent border element) are used to allow the flow to transfer into or out of the domain. Figure 8a shows the free surface elevation at the shoreline ($\eta(x_s(y,t))$) at the time of maximum run-up and run-down over the whole domain during the tenth period of the simulation (solid lines) and also at the 200th period of the simulation (dashed lines). It

can be seen that an oscillation of wavelength λ has developed. The transition from the first state to the second can be seen in Figure 8b, in which $\eta(x = 94m,\ y = 31.215m,\ t)$ is plotted. It also can be noticed that the instability appears to start developing at $t \approx 500$s, and develops over about 1250 s, after which time it has equilibrated. Figures 8a,b together imply the development of an alongshore periodic motion at the subharmonic wavelength, and therefore the successful reproduction of the edge wave mechanism.

This behaviour is similar to that observed by Özkan-Haller and Kirby (1997), who went further and considered the detuning of the generation process (i.e. variation of the incoming wave period such that λ no longer corresponds to a wavelength that is unstable). They considered the detuning parameter Δ of Rockliff (1978), such that

$$\frac{\omega_i}{2} = (1 + 0.0338\epsilon_i\Delta)\omega\,, \tag{35}$$

which relates incident angular frequency ω_i to the edge wave angular frequency ω, where $\epsilon_i = \epsilon_i(a_i, \omega_i, \beta)$. Figure 9 shows examples of the development of the sub-harmonic edge wave for various Δ values ($\Delta = -0.9,\ 0,\ 1$). It is clear that the case of $\Delta = 0$ has the fastest sub-harmonic edge wave development and is the first to reach steady state, which is consistent with the findings of Özkan-Haller and Kirby (1997). In the present simulation, for $\Delta = 0$ the flow reaches steady state (i.e., equilibration) around $t = 1700$s, while for Özkan-Haller and Kirby (1997) for the same Δ the flow did so after $t = 2000$s. For $\Delta = 1, -0.9$ the present model simulations reach steady state after $t = 3000, 1800$s respectively, while Özkan-Haller and Kirby (1997) simulation for $\Delta = 0.96, -0.98$ equilibrated after $t = 4700, 4000$s respectively. It therefore seems that the present model reaches steady state significantly faster. It seems likely that this is due to the larger a_i used here. It should also be noted that Özkan-Haller and Kirby (1997) utilised an initial perturbation at the edge wave wavelength of amplitude 1 mm. It is not clear how much their results depend on this initial perturbation, and whether the present larger initial incident wave amplitude mimics this effect. Rockliff (1978) was also able to find a relationship between the fully developed edge wave

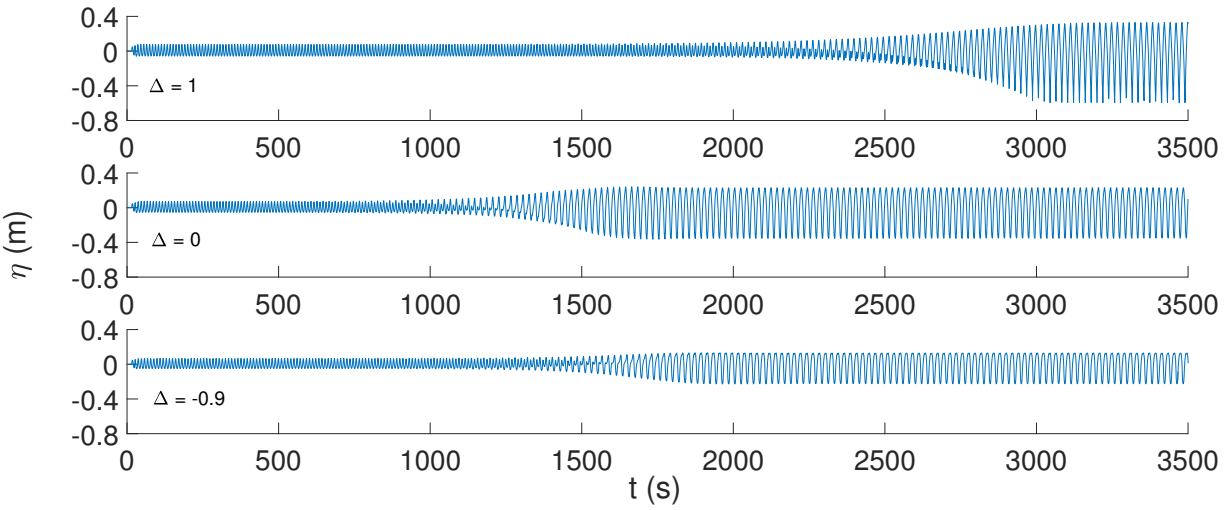

Fig. 9. η at 6 m away from still water shoreline for various values of Δ.

amplitude a and Δ (Figure 10 - solid line). Numerical experiments were carried out for a number of Δ values both within and outside the region in which resonance should occur. It can be seen that the present simulation (Figure 10 - black dots) agrees fairly well with the Rockliff curve. The results of Özkan-Haller and Kirby (1997) are closer to the analytical curve. Their approach made use of mapping the moving shoreline onto a fixed grid, which can be expected to be more accurate compared to a fixed mesh wetting/drying approach like that used here (see also Huynh et al. 2017). Overall the correspondence follows the expected behaviour of a as function of Δ and increases up to $\Delta = 1$.

CONCLUSIONS

The accuracy of a new 2D DGFEM model for solving the NSWEs for a number of swash flows has been analysed. This model, which is based mostly on existing DGFEM techniques, augmented by a new wetting/drying algorithm, provides accurate modelling for; three classical and demanding test cases for swash flows (CG58, PW01, Özkan-Haller and Kirby 1997), two less explored and demanding test cases (Antuono 2010, Zhu and Dodd 2015), and a flow demanding of good swash modelling for successful reproduction (Thacker 1981, see Appendix). Only two of these flows have previously been reproduced using DGFEMs: the periodic solution of CG58, by Bunya et al. (2009); and the rotating bowl of water with constant free surface gradient constant of Thacker (1981) (see

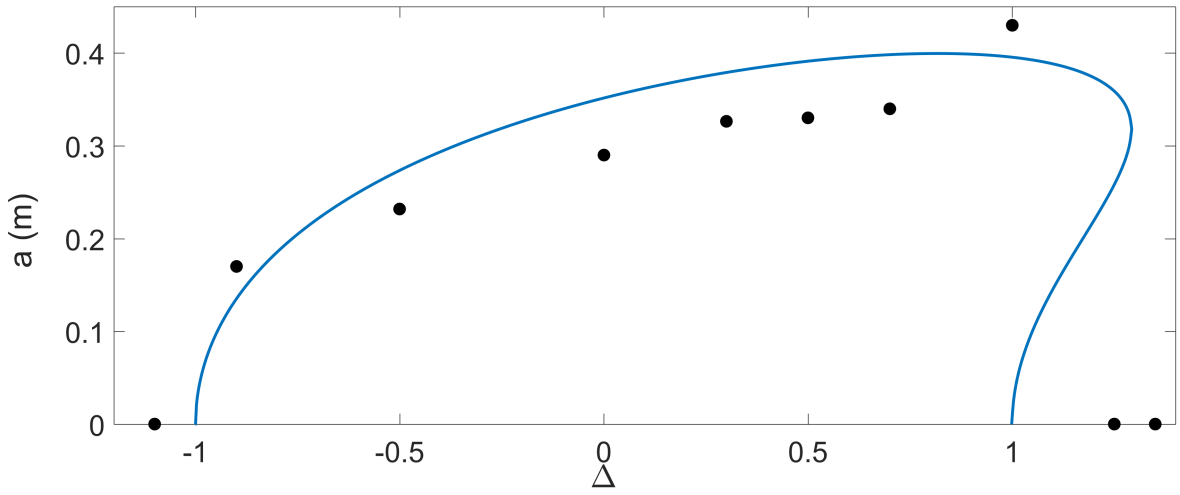

Fig. 10. Edge wave amplitude versus detuning parameter Δ, analytical (blue line), DGFEM (black dots). Note that the apparently dual-valued region of the figure in fact corresponds to distinct phase differences between incident and edge waves, which do not show here (Özkan-Haller and Kirby 1997; Rockliff 1978).

Appendix), by Duran et al. (2013) (who only show water depth, not velocity). Together with the bore collapse solution of Shen and Meyer (1963), the shock solution of Antuono (2010), the solitary wave over frictional bed case, and the subharmonic edge wave generation solution first elucidated by Guza and Davis (1974), which have never before been examined using DGFEM, they illustrate the viability of DGFEM methods for swash type problems.

Note that results presented here are for first order time integration and first order shape functions. Other authors (e.g. Bunya et al. 2009; Brus et al. 2019; Ern et al. 2008) have examined higher order time integration, or higher order shape functions (e.g. Kubatko et al. 2006; Giraldo et al. 2002). There is clearly scope for improving efficiency in swash problems, but note in particular that the relatively dissipative approach still captures the subharmonic generation process.

The proposed wetting/drying algorithm gives good performance, particularly as shown in the comparison against a state-of-the-art finite volume solver (Briganti and Dodd 2009) for the demanding bore collapse case and against similar wetting/drying algorithm of Bunya et al. (2009) for the solitary wave over frictional bed case. $h_{min} = 10^{-3}$ m was chosen as a starting value because it was used in field applications in the context of FVM models (e.g. Incelli et al. 2016). Also, it

was found that for a specific element size there is an approximate minimum h_{min} that is optimal. In most cases the ratio $h_{min}/\Delta x$ was around $1/10$. Lower water depth gradient at the shoreline $dh(x_s)/dx$ would also tend to lower this value, and vice versa.

The model is non-dissipative enough to simulate more subtle processes such as sub-harmonic edge wave excitation and development. The results are, overall, qualitatively and quantitatively similar to those of Özkan-Haller and Kirby (1997), who used more accurate approach to resolving the shoreline motion. The relatively fast evolution to the steady state achieved here is, as noted, probably due to using larger dimensional wave amplitude compared to the one used by Özkan-Haller and Kirby (1997).

Overall the results shown demonstrate that the present model, including the wetting/drying treatment, is applicable to idealised and realistic waves. The second order RK time integration showed excessive noise at the water front when applied to the PW01 verification test only, even when using Bunya et al. (2009) algorithm. Switching to first order Euler time integration removes this problem at the expense of losing second order accuracy. This, in addition to being non-conservative, wetting/drying algorithm needs further study to overcome these constraints.

APPENDIX

Spinning water in a parabolic bowl

This case, due to Thacker (1981), is a useful one, because it is very demanding. It comprises a circle of water (viewed from above) with a free surface of constant gradient travelling in a circle around the centre of a bowl with constant angular velocity and without change of shape. It is one of a family of solutions presented by Thacker (1981). Strictly speaking it is not a swash event, but is a demanding test (Hubbard and Dodd 2002) of a 2D model because of the wetting and drying and the symmetry, which can reveal anomalies in the modelling.

The solution is periodic and should return to its initial conditions after any integer number of periods. The bowl bed (parabola) is given by $z_b = z_o(1 - (x^2 + y^2)/L^2)$, which leads to analytical,

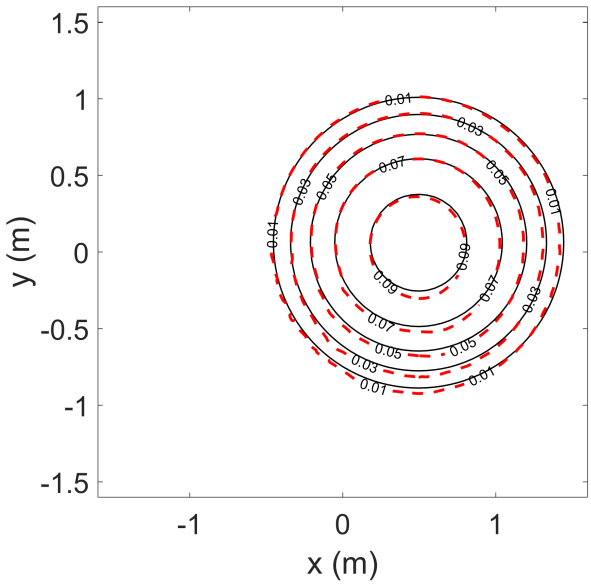

Fig. 11. Thacker (1981), h contours; comparison between DGFEM (red dashed lines) and analytical solution (black lines) after one complete revolution.

periodic solution of the form,

$$\eta = \frac{\eta_o z_o}{L^2}(2x\cos(\omega t) + 2y\sin(\omega t) - \eta_o), \tag{36}$$

$$u = -\eta_o \omega \sin(\omega t), \tag{37}$$

$$v = -\eta_o \omega \cos(\omega t), \tag{38}$$

where $\omega = \sqrt{2gh_o}/L$, and the free parameters are chosen to be $z_o = -0.1$m, $\eta_o = 0.5$m, $L = h_o = 1$m. It is therefore identical to the case examined by Hubbard and Dodd (2002). The solution at $t = 0$s was used as the initial condition. The domain is discretized into 623336 triangular elements ($\Delta x \approx \Delta y \approx 0.0045$m), and the minimum threshold for the drying was set to $h_{min} = 10^{-3}$m. A larger h_{min} and element size are used here because $dh(x_s)/dx \neq 0$, so the shoreline modelling is not so demanding as in the case of PW01. A complete period of 4.4s is simulated. Figures 11 and 12a show that the model gives a generally accurate reproduction of h after one complete revolution with RMS error of 0.0022m for the Figure 12a. Reproduction of velocities is the most demanding aspect of this test, as can be seen in Figure 12b. These velocity predictions have RMS error of

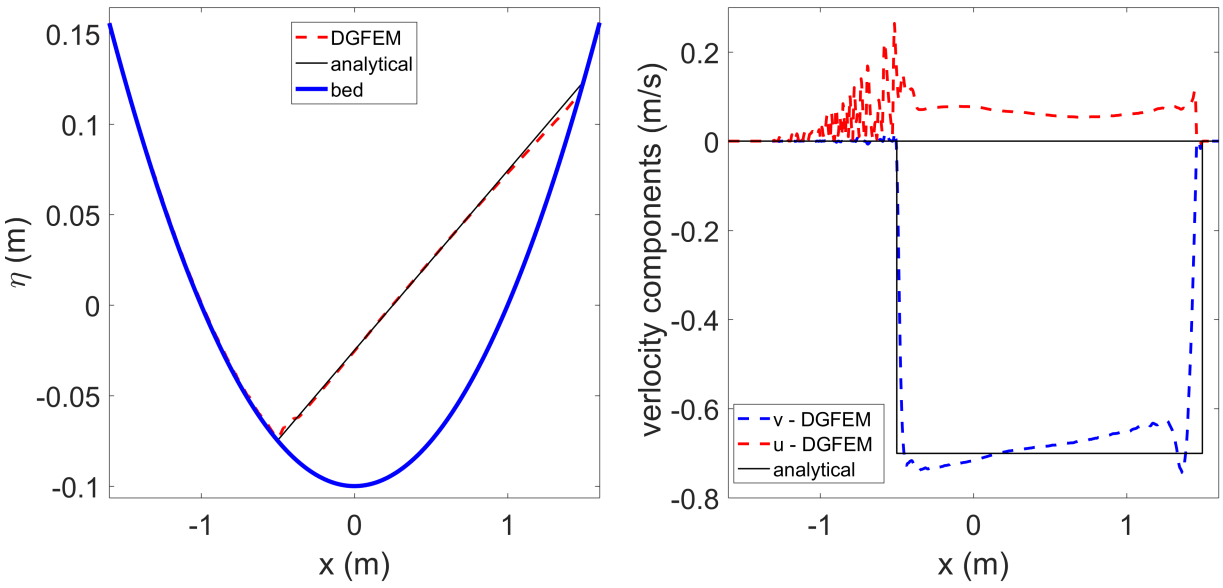

(a) **(b)**

Fig. 12. Thacker (1981); comparison between DGFEM and analytical solution after one complete revolution, (a)η, (b)u, v.

0.0657m/s for u and 0.1036m/s for v. The accuracy obtained is qualitatively and quantitatively similar to that obtained by Hubbard and Dodd (2002) (using FVM). Duran et al. (2013) examine a problem similar to the present one, using DGFEM, albeit with different parameters. They achieve similar accuracy in terms of free surface elevation but do not show the accompanying velocities.

DATA AVAILABILITY

The following data, models, or code generated or used during the study are available from the corresponding author by request:

- DGFEM model code.
- The model results for the periodic solution of the Carrier-Greenspan (1958).
- The model results for the case of bore collapse at the shoreline.
- The model results for the case of the shock solution of Antuono (2010).
- The model results for the case of the solitary wave over a frictional beach.
- The model results for the case of the sub-harmonic edge wave generation.

ACKNOWLEDGEMENTS

This research is sponsored by Newton-Mosharafa scholarship programme. The authors would like to thank the University of Nottingham for using its High Performance Computer (HPC), which allowed the use of parallel processing over both CPU and GPU. The authors also would like to thank Dr. FangFang Zhu for providing the quasi-analytical solution data for the solitary wave case.

REFERENCES

Aizinger, V. and Dawson, C. (2002). "A discontinuous Galerkin method for two-dimensional flow and transport in shallow water." *Advances in Water Resources*, 25(1), 67–84.

Antuono, M. (2010). "A shock solution for the nonlinear shallow water equations." *Journal of Fluid Mechanics*, 658, 166–187.

Bakhtyar, R., Barry, D. A., Li, L., Jeng, D. S., and Yeganeh-Bakhtiary, A. (2009). "Modeling sediment transport in the swash zone: A review." *Ocean Engineering*, 36(9–10), 767–783.

Baldock, T. E. and Holmes, P. (1999). "Simulation and prediction of swash oscillations on a steep beach." *Coastal Engineering*, 36, 219–242.

Borthwick, A. G. L., Ford, M., Weston, B. P., Taylor, P. H., and Stansby, P. K. (2006). "Solitary wave transformation, breaking and run-up at a beach." *Proceedings of the Institution of Civil Engineers - Maritime Engineering*, 159(3), 97–105.

Briganti, R. and Dodd, N. (2009). "Shoreline motion in nonlinear shallow water coastal models." *Coastal Engineering*, 56(5), 495–505.

Briganti, R., Torres-Freyermuth, A., Baldock, T., Brocchini, M., Dodd, N., Hsu, T.-J., Jiang, Z., Kim, Y., Pintado-Patiño, J., and Postacchini, M. (2016). "Advances in numerical modelling of swash zone dynamics." *Coastal Engineering*, 115, 26–41.

Briggs, M. J., Synolakis, C. E., Harkins, G. S., and Green, D. R. (1995). "Laboratory experiments of tsunami run-up on circular island." *Pure and Applied Geophysics*, 144(3/4), 569–593.

Brocchini, M., Bernetti, R., Mancinelli, A., and Albertini, G. (2001). "An efficient solver for nearshore flows based on the waf method." *Coastal Engineering*, 43(2), 105 – 129.

Brus, S. R., Wirasaet, D., Kubatko, E. J., Westerink, J. J., and Dawson, C. (2019). "High-order

discontinuous Galerkin methods for coastal hydrodynamics applications." *Computer Methods in Applied Mechanics and Engineering*, 355, 860 – 899.

Bunya, S., Kubatko, E. J., Westerink, J. J., and Dawson, C. (2009). "A wetting and drying treatment for the Runge-Kutta discontinuous Galerkin solution to the shallow water equations." *Computer Methods in Applied Mechanics and Engineering*, 198(17–20), 1548–1562.

Carrier, G. F. and Greenspan, H. P. (1958). "Water waves of finite amplitude on a sloping beach." *Journal of Fluid Mechanics*, 4(1), 97–109.

Chardón-Maldonado, P., Pintado-Patiño, J. C., and Puleo, J. A. (2016). "Advances in swash-zone research: Small-scale hydrodynamic and sediment transport processes." *Coastal Engineering*, 115, 8–25.

Dawson, R. J., Peppe, R., and Wang, M. (2011). "An agent-based model for risk-based flood incident management." *Natural Hazards*, 59, 167–189.

de Brye, B., de Brauwere, A., Gourgue, O., Karna, T., Lambrechts, J., Comblen, R., and Deleersnijder, E. (2010). "A finite-element, multi-scale model of the Scheldt tributaries, river, estuary and ROFI." *Coastal Engineering*, 57(9), 850 – 863.

Duran, A., Liang, Q., and Marche, F. (2013). "On the well-balanced numerical discretization of shallow water equations on unstructured meshes." *Journal of Computational Physics*, 235, 565–586.

Duran, A. and Marche, F. (2014). "Recent advances on the discontinuous Galerkin method for shallowwater equations with topography source term." *Computers and Fluids*, 101, 88–104.

Ern, A., Piperno, S., and Djadel, K. (2008). "A well-balanced Runge–Kutta discontinuous Galerkin method for the shallow-water equations with flooding and drying." *International Journal for Numerical Methods in Fluids*, 58, 1–25.

Giraldo, F. X., Hesthaven, J. S., and Warburton, T. (2002). "Nodal high-order discontinuous Galerkin methods for the spherical shallow water equations." *Journal of Computational Physics*, 181, 499–525.

Gourgue, O., Comblen, R., Lambrechts, J., Karna, T., Legat, V., and Deleersnijder, E. (2009). "A

flux-limiting wetting–drying method for finite-element shallow-water models, with application to the Scheldt Estuary." *Advances in Water Resources*, 32, 1726–1739.

Guza, R. T. and Davis, R. E. (1974). "Excitation of edge waves by waves incident on a beach." *Journal of Geophysical Research*, 79(9), 1285–1291.

Harten, A. (1983). "High resolution schemes for hyperbolic conservation laws." *Journal of Computational Physics*, 49(3), 357–393.

Hubbard, M. E. and Dodd, N. (2002). "A 2D numerical model of wave run-up and overtopping." *Coastal Engineering*, 47(1), 1–26.

Huynh, V. L., Dodd, N., and Zhu, F. (2017). "Coastal morphodynamical modelling in nonlinear shallow water framework using a coordinate transformation method." *Advances in Water Resources*, 107, 326–335.

Incelli, G., Dodd, N., Blenkinsopp, C. E., Zhu, F., and Briganti, R. (2016). "Morphodynamical modelling of field-scale swash events." *Coastal Engineering*, 115, 42–57 Swash-zone Processes.

Karna, T., de Brye, B., Gourgue, O., Lambrechts, J., Comblen, R., Legat, V., and Deleersnijder, E. (2011). "A fully implicit wetting–drying method for DG-FEM shallow water models, with an application to the Scheldt Estuary." *Computer Methods in Applied Mechanics and Engineering*, 200, 509–524.

Kesserwani, G., Ayog, J. L., and Bau, D. (2018). "Discontinuous Galerkin formulation for 2D hydrodynamic modelling: Trade-offs between theoretical complexity and practical convenience." *Computer Methods in Applied Mechanics and Engineering*, 342, 710–741.

Kesserwani, G. and Liang, Q. (2010). "Well-balanced RKDG2 solutions to the shallow water equations over irregular domains with wetting and drying." *Computers and Fluids*, 39, 2040–2050.

Kobayashi, N. ., Otta, A. K., and Roy, I. (1987). "Wave reflection and runup on rough slopes." *Journal of Waterway, Port, Coastal, and Ocean Engineering*, 113(3), 282–298.

Kubatko, E. J., Bunya, S., Dawson, C., Westerink, J. J., and Mirabito, C. (2009). "A performance comparison of continuous and discontinuous finite element shallow water models." *Journal of*

Scientific Computing, 40(1), 315–339.

Kubatko, E. J., Westerink, J. J., and Dawson, C. (2006). "*hp* Discontinuous Galerkin Methods for Advection Dominated Problems in Shallow Water Flow." *Computer Methods in Applied Mechanics and Engineering*, 196(1-3), 437–451.

Lai, W. and Khan, A. A. (2012). "Discontinuous Galerkin method for 1D shallow water flows in natural rivers." *Engineering Applications of Computational Fluid Mechanics*, 6(1), 74–86.

Le Bars, Y., Vallaeys, V., Deleersnijder, J., Hanert, E., Carrere, L., and Channeliere, C. (2016). "Unstructured-mesh modeling of the Congo river-to-sea continuum." *Ocean Dynamics*, 66, 589–603.

Lee, H. and Lee, N. (2016). "Wet-dry moving boundary treatment for Runge-Kutta discontinuous Galerkin shallow water equation model." *KSCE Journal of Civil Engineering*, 20(2), 978–989.

LeVeque, R. J. (2002). *Finite Volume Methods for Hyperbolic Problems*. Cambridge Texts in Applied Mathematics. Cambridge University Press.

Li, B. Q. (2006). *Discontinuous Finite Elements in Fluid Dynamics and Heat Transfer*. Computational Fluid and Solid Mechanics. Springer-Verlag London.

Marras, S., Kopera, M. A., Constantinescu, E. M., Suckale, J., and Giraldo, F. X. (2018). "A residual-based shock capturing scheme for the continuous/discontinuous spectral element solution of the 2D shallow water equations." *Advances in Water Resources*, 114, 45–63.

Mase, H. (1995). "Frequency down-shift of swash oscillations compared to incident waves." *Journal of Hydraulic Research*, 33(3), 397–411.

Mulamba, T., Bacopoulos, P., Kubatko, E. J., and Pinto, G. F. (2019). "Sea-level rise impacts on longitudinal salinity for a low-gradient estuarine system." *Climatic Change*, 152, 533–550.

Özkan-Haller, H. T. and Kirby, J. T. (1997). "A Fourier-Chebyshev collocation method for the shallow water equations including shoreline runup." *Applied Ocean Research*, 19(1), 21–34.

Peregrine, D. H. and Williams, S. M. (2001). "Swash overtopping a truncated plane beach." *Journal of Fluid Mechanics*, 440, 391–399.

Pritchard, D. and Hogg, A. J. (2003). "Cross-shore sediment transport and the equilibrium mor-

phology of mudflats under tidal currents." *Journal of Geophysical Research: Oceans*, 108(C10).

Rockliff, N. (1978). "Finite amplitude effects in free and forced edge waves." *Mathematical Proceedings of the Cambridge Philosophical Society*, Vol. 83, Cambridge University Press, 463–479.

Roe, P. (1981). "Approximate Riemann solvers, parameter vectors, and difference schemes." *Journal of Computational Physics*, 43(2), 357–372.

Rogers, B., Borthwick, A., and Taylor, P. (2003). "Mathematical balancing of flux gradient and source terms prior to using Roe's approximate Riemann solver." *Journal of Computational Physics*, 192, 422–451.

Shen, M. C. and Meyer, R. E. (1963). "Climb of a bore on a beach Part 3. Run-up." *Journal of Fluid Mechanics*, 16(1), 113–125.

Thacker, W. C. (1981). "Some exact solutions to the nonlinear shallow-water wave equations." *Journal of Fluid Mechanics*, 107(-1), 499.

Wen, X., Gao, Z., Don, W. S., Xing, Y., and Li, P. (2016). "Application of positivity-preserving well-balanced discontinuous Galerkin method in computational hydrology." *Computers & Fluids*, 139, 112–119.

Zelt, J. A. (1986). "Tsunamis: the response of harbors with sloping boundaries to long wave excitation." *Report No. KH-R-47*, California Institute of Technology.

Zhu, F. and Dodd, N. (2013). "Net beach change in the swash zone: A numerical investigation." *Advances in Water Resources*, 53, 12–22.

Zhu, F. and Dodd, N. (2015). "The morphodynamics of a swash event on an erodible beach." *Journal of Fluid Mechanics*, 762, 110–140.